ON THE INITIAL RELATIVE WIND DIRECTION OF DYNAMIC SOARING

A. Zwenig, H. Hong, F. Holzapfel
Technical University of Munich, TUM School of Engineering and Design, Department of Aerospace and Geodesy, Institute of Flight System Dynamics, 85748 Garching bei München, Germany

Abstract

For enhancing the range and endurance of Remotely Piloted Aircraft Systems (RPAS), vertical wind shears can be utilized to extract energy from the environment. This technique, known as dynamic soaring, can be observed in large seabirds, e.g. albatrosses. The natural variation of the environment requires a profound understanding of how the wind field parameters like wind direction and wind speed affect the dynamic soaring capability. Therefore, this study illuminates the influence of the initial relative wind direction on the dynamic soaring performance. With the help of direct optimal control methods, the minimum required wind speed is quantified, which is an important criterion for energy extraction performance. The results reveal favorable and unfavorable initial relative wind directions. Furthermore, detailed insights into the sensitivity of the minimum required wind speed and the travel direction with respect to the initial relative wind direction are given. Thereof, operational requirements of potential RPAS performing dynamic soaring can be derived. The results are of guiding value for RPAS operations, offering direct and pertinent information to steer the mission planning.

Keywords

Dynamic Soaring; Trajectory Optimization; Optimal Control

1. INTRODUCTION

Enroute, albatrosses hardly require to flap their wings as they extract energy from the wind to compensate for the energy dissipation due to aerodynamic drag [1, 2]. This flight technique is known as dynamic soaring. If the extracted energy equals the dissipated energy, an energy-neutral dynamic soaring cycle is achieved. This enables to cover large distances comparatively fast and nearly effortless [3, 4]. The transfer of this principle to aircraft systems offers the potential for more ecological and economical aircraft operations in the future. To demonstrate the practicability, small scale Remotely Piloted Aircraft Systems (RPAS) may be used. Therefore a profound understanding of the flight physics of dynamic soaring is necessary. Optimal control is widely used to analyze the characteristics of dynamic soaring [5–8]. The energy transfer between the wind and the bird was examined in [6, 9], considering different reference frames. Bousquet et al. [8] studied the influence of the shear layer thickness on the shape of a minimum wind cycle and compared their observations to logged flight data of wandering albatrosses from [3, 4]. In [7] Flanzer et al. investigated the sensitivity of the energy at the end of a cycle and of the altitude along the trajectory with respect to aircraft properties, environmental parameters, and initial conditions. In [5, 10] Sachs studied the minimum required wind shear strength for an energy-neutral dynamic soaring cycle. The minimum required wind strength is of particular importance for planning the optimal dynamic soaring trajectory to be followed. However, the influence of the relative wind direction on such a criterion is unknown, and yet it is crucial as the current aircraft state and wind conditions determine the optimal dynamic soaring trajectory. Hence, to gain further insights on the influence of the wind conditions on the requirements of dynamic soaring, in this study the authors illuminate the influence of the initial relative wind direction. To this end, we quantify the minimum required wind speed to perform an energy-neutral dynamic soaring cycle in different conditions. These results become particularly important for trajectory planning tasks as the current aircraft state and wind conditions determine the optimal trajectory to be followed. We analyze the wind speed requirement by solving a series of parametric optimal control problems with varying initial relative wind directions. Note that energy-neutrality refers to the total mechanical energy only, and does not include energy demands due to onboard systems, such as sensors, actuators, and control computers. The optimal control problems are solved with FALCON.m [11]. Thereby, the problem is discretized first and then transcribed into a nonlinear program which is solved by the interior point optimizer IPOPT [12]. The structure of this work is as follows: Section 2 outlines the aircraft model and the point mass equations of motion (EoM). In section 3 the nominal optimal control problem is formulated. In section 4 a modification to the nominal problem to model varying initial relative wind directions is presented. Subsequently, the results are presented and a discussion of the influence of differ-

doi: 10.25967/570157

ent initial relative wind directions on an energy-neutral dynamic soaring cycle succeeds. The conclusion follows in section 5.

2. AIRCRAFT MODEL

This section presents the aircraft model including its equations of motion, aerodynamics, and the wind model. For the aircraft, a model fidelity with three degrees of freedom is considered. The atmosphere is based on the standard atmosphere [13] at sea level; the change of atmospheric conditions with height is neglected. This assumption is justified since the aircraft operates in close vicinity to the surface. The state vector of the aircraft, $\boldsymbol{x} \in \mathbb{R}^{6\times1}$, comprises its position and inertial velocity:

$$\boldsymbol{x} = \begin{bmatrix} x_N & y_N & z_N & V_K & \chi_K & \gamma_K \end{bmatrix}^\mathsf{T}. \tag{1}$$

The aircraft's controls $\boldsymbol{u} \in \mathbb{R}^{2\times1}$ are the lift coefficient C_L and the aerodynamic bank angle μ_A:

$$\boldsymbol{u} = \begin{bmatrix} C_L & \mu_A \end{bmatrix}^\mathsf{T}. \tag{2}$$

Sections 2.1 to 2.4 outline the model in detail. Table 1 gives an overview of the model data.

2.1. Equations of Motion

The model is derived under the simplifying assumptions of a non-rotating and flat earth. These are justified as the aircraft operates at relatively low speeds and covers only small distances. The position is specified in a local north-east-down (NED) coordinate frame denoted by $(\cdot)_N$:

$$\begin{aligned} \dot{x}_N &= V_K cos(\gamma_K) cos(\chi_K) \\ \dot{y}_N &= V_K cos(\gamma_K) sin(\chi_K) \\ \dot{z}_N &= -V_K sin(\gamma_K). \end{aligned} \tag{3}$$

The kinematic velocity is denoted by $(\cdot)_K$:

$$\begin{aligned} \dot{V}_K &= \frac{(X_T)_K}{m} \\ \dot{\chi}_K &= \frac{(Y_T)_K}{m V_K cos(\gamma_K)} \\ \dot{\gamma}_K &= -\frac{(Z_T)_K}{m V_K}. \end{aligned} \tag{4}$$

The total force acting on the aircraft comprises aerodynamic and gravitational forces, $\boldsymbol{F}_A$ and $\boldsymbol{F}_G$:

$$(\boldsymbol{F}_T)_K = \begin{bmatrix} X_T \\ Y_T \\ Z_T \end{bmatrix}_K = (\boldsymbol{F}_A)_K + (\boldsymbol{F}_G)_K. \tag{5}$$

The gravitational force in the kinematic frame is obtained by:

$$(\boldsymbol{F}_G)_K = \boldsymbol{T}_{KN} \begin{bmatrix} 0 \\ 0 \\ mg_0 \end{bmatrix}_N. \tag{6}$$

The transformation matrix $\boldsymbol{T}_{KN}(\chi_K, \gamma_K)$ can be found in appendix A.

2.2. Wind Model

As in [5, 6, 9], we assume a logarithmic wind shear profile. Thus, the wind speed is obtained as a function of the height above surface $h = -z_N$:

$$V_W = V_{W,ref} \frac{\ln(h/h_0)}{\ln(h_{ref}/h_0)}. \tag{7}$$

The surface roughness h_0 and the reference height h_{ref} influence the shape of the wind profile. The reference wind speed $V_{W,ref}$, specified at h_{ref} determines the wind strength and wind gradient of the wind field.

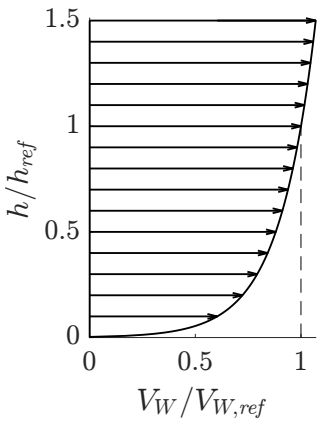

FIG 1. Logarithmic wind profile according to [5].

Figure 1 illustrates the wind profile. The wind velocity in local NED coordinates is:

$$\boldsymbol{v}_W = \begin{bmatrix} V_W & 0 & 0 \end{bmatrix}_N^\mathsf{T}. \tag{8}$$

2.3. Aerodynamics

From the wind triangle we obtain the aerodynamic velocity:

$$\boldsymbol{v}_A = \boldsymbol{v}_K - \boldsymbol{v}_W = \begin{bmatrix} u_A & v_A & w_A \end{bmatrix}^\mathsf{T} \tag{9}$$

and consequentially the air speed:

$$V_A = \sqrt{u_A^2 + v_A^2 + w_A^2}. \tag{10}$$

The lift coefficient C_L is chosen as control variable. For the drag coefficient we assume a quadratic polar:

$$C_D = C_{D0} + k C_L^2. \tag{11}$$

The aerodynamic lift and drag forces L and D are specified by:

$$L = \frac{1}{2}\rho V_A^2 S C_L \qquad D = \frac{1}{2}\rho V_A^2 S C_D. \tag{12}$$

The aerodynamic side force Q is assumed to be negligible. The total aerodynamic force is then transformed into the kinematic frame by

$$(\boldsymbol{F}_A)_K = \boldsymbol{T}_{KA}\,(\boldsymbol{F}_A)_A = \boldsymbol{T}_{KA}\begin{bmatrix}-D\\0\\-L\end{bmatrix}_A \tag{13}$$

and

$$\boldsymbol{T}_{KA} = \boldsymbol{T}_{KN}\,\boldsymbol{T}_{NA}. \tag{14}$$

The transformation matrix $\boldsymbol{T}_{NA}(\chi_A, \gamma_A, \mu_A)$ can be found in appendix A.

2.4. Model Data

The model data is specified in table 1 and is based on the albatross and wind model used by Sachs in [5].

TAB 1. Model data

Parameter	Symbol	Value	
Aircraft data			
Mass	m	8.5	kg
Wing reference area	S	0.65	m^2
Wing span	b	3.44	m
Max. lift coefficient	$C_{L,max}$	1.5	-
Zero-lift drag coefficient	$C_{D,0}$	0.033	-
Lift-dependant drag factor	k	0.019	-
Environmental data			
Air density	ρ	1.225	kgm^{-3}
Gravitational acceleration	g_0	9.81	ms^{-2}
Wind reference height	h_{ref}	10	m
Surface roughness	h_0	0.03	m

We can compute the stall speed from the model data as follows:

$$V_{stall} = \sqrt{\frac{2mg_0}{\rho S C_{L,max}}} = 11.81\,\mathrm{m\,s^{-1}}. \tag{15}$$

3. NOMINAL OPTIMAL CONTROL PROBLEM

To analyze the influence of the initial relative wind direction on the requirements for an energy-neutral dynamic soaring cycle, the following parametric optimal control problem is solved on the interval $t \in [t_0, t_f]$:

$$\begin{aligned}
\min_{\boldsymbol{u}(t),\boldsymbol{x}(t),\boldsymbol{p}} \quad & J \\
\text{subject to} \quad & \dot{\boldsymbol{x}}(t) = \boldsymbol{f}(\boldsymbol{x}(t), \boldsymbol{u}(t), \boldsymbol{p}) \\
& \boldsymbol{x}_{lb} \le \boldsymbol{x}(t) \le \boldsymbol{x}_{ub} \\
& \boldsymbol{u}_{lb} \le \boldsymbol{u}(t) \le \boldsymbol{u}_{ub} \\
& \boldsymbol{p}_{lb} \le \boldsymbol{p}(t) \le \boldsymbol{p}_{ub} \\
& \boldsymbol{\psi}_x(\boldsymbol{x}(t_0), \boldsymbol{x}(t_f)) = \boldsymbol{0} \\
& \boldsymbol{\psi}_u(\boldsymbol{u}(t_0), \boldsymbol{u}(t_f)) = \boldsymbol{0}.
\end{aligned} \tag{16}$$

To quantify the minimum wind requirement for an energy-neutral cycle we seek to minimize the reference wind speed:

$$J = V_{W,ref}. \tag{17}$$

States and controls were given in (1) and (2). We obtain the nonlinear state dynamics $\boldsymbol{f} : \mathbb{R}^{6\times1} \times \mathbb{R}^{2\times1} \times \mathbb{R}^{2\times1} \to \mathbb{R}^{6\times1}$ from the state derivatives in (3) and (4):

$$\boldsymbol{f}(\boldsymbol{x}(t), \boldsymbol{u}(t), \boldsymbol{p}) = \begin{bmatrix}\dot{x}_N & \dot{y}_N & \dot{z}_N & \dot{V}_K & \dot{\chi}_K & \dot{\gamma}_K\end{bmatrix}^\mathsf{T}. \tag{18}$$

To compensate for the negligence of modeling the rotational dynamics and yet still account for the capabilities of a physical system, control rate limits are imposed:

$$\begin{aligned}
-2\,\mathrm{s^{-1}} \le \dot{C}_L \le 2\,\mathrm{s^{-1}} \\
-2\,\mathrm{rad\,s^{-1}} \le \dot{\mu}_A \le 2\,\mathrm{rad\,s^{-1}}.
\end{aligned} \tag{19}$$

Thereby, erratic controls, numerical chattering, and solutions with high-frequency control activity are prevented. Such chattering would exert high loads on the actuators and potentially damage the system. Also, increasing control activities entail higher onboard power consumption. This is particularly undesirable for our application, which aims at minimizing the use of onboard energy resources, while extracting energy from the wind for propelling the system.
Problem parameters $\boldsymbol{p} \in \mathbb{R}^{2\times1}$ are subject to optimization and given by:

$$\boldsymbol{p} = \begin{bmatrix}V_{W,ref} & t_f\end{bmatrix}^\mathsf{T}. \tag{20}$$

Box constraints guarantee that the resulting trajectory remains within the performance limits of the aircraft. The lower (LB) and upper bounds (UB) can be found in table 2. To avoid convergence issues originating from singularities in (4) induced by γ_K approaching $\pm90°$, LB and UB are enforced. Since ground speeds close to $V_K = 0\,\mathrm{m\,s^{-1}}$ are not purposeful, an additional restriction was not necessary. To avoid impact on the surface, the z_N-coordinate is upper bounded to $z_0 = -1\,m$. The upper bound for the final time t_f excludes multiple consecutive cycles from the

TAB 2. State, control, and parameter bounds.

LB		Variable		UB
		States		
$-\infty$	$\leq$	x_N	$\leq$	∞
$-\infty$	$\leq$	y_N	$\leq$	∞
$-\infty$	$\leq$	z_N	$\leq$	z_0
0	$\leq$	V_K	$\leq$	∞
$-\infty$	$\leq$	χ_K	$\leq$	∞
$-80°$	$\leq$	γ_K	$\leq$	$80°$
		Controls		
0	$\leq$	C_L	$\leq$	$C_{L,max}$
$-80°$	$\leq$	μ_A	$\leq$	$80°$
		Parameters		
0	$\leq$	$V_{W,ref}$	$\leq$	∞
0	$\leq$	t_f	$\leq$	$10\,s$

solution space.

To impose energy-neutral dynamic soaring, the mechanical energy after the cycle is enforced to equal the energy at the start of the cycle by the state boundary constraints $\boldsymbol{\psi}_x : \mathbb{R}^{6\times1} \times \mathbb{R}^{6\times1} \rightarrow \mathbb{R}^{7\times1}$:

$$\boldsymbol{\psi}_x(\boldsymbol{x}(t_0), \boldsymbol{x}(t_f)) = \begin{bmatrix} x_N(t_0) \\ y_N(t_0) \\ z_N(t_0) - z_0 \\ z_N(t_0) - z_N(t_f) \\ V_K(t_0) - V_K(t_f) \\ \chi_K(t_0) - \chi_K(t_f) \\ \gamma_K(t_0) - \gamma_K(t_f) \end{bmatrix} = \mathbf{0}. \tag{21}$$

We constrain the initial lateral position without any loss of generality to coincide with the origin of the local NED coordinate frame. The initial z_N-coordinate is set to its upper bound of $z_0 = -1\,m$. To ensure periodicity of the maneuver, the controls at the start and end of the cycle are synchronized by the control boundary constraints $\boldsymbol{\psi}_u : \mathbb{R}^{2\times1} \times \mathbb{R}^{2\times1} \rightarrow \mathbb{R}^{2\times1}$:

$$\boldsymbol{\psi}_u(\boldsymbol{u}(t_0), \boldsymbol{u}(t_f)) = \begin{bmatrix} C_L(t_0) - C_L(t_f) \\ \mu_A(t_0) - \mu_A(t_f) \end{bmatrix} = \mathbf{0}. \tag{22}$$

The described optimal control problem was solved with FALCON.m [11] which uses direct optimization methods with full state and control discretization [14, 15]. The solution of the nominal result is compared to head-, tail-, and crosswind conditions in the subsequent section.

4. INFLUENCE OF THE INITIAL RELATIVE WIND DIRECTION

To investigate the influence of the initial relative wind direction, the nominal optimal control problem from section 3 is slightly modified. The state boundary constraints in (21) are replaced by:

$$\boldsymbol{\psi}_x(\boldsymbol{x}(t_0), \boldsymbol{x}(t_f)) = \begin{bmatrix} x_N(t_0) \\ y_N(t_0) \\ z_N(t_0) - z_0 \\ z_N(t_0) - z_N(t_f) \\ V_K(t_0) - V_K(t_f) \\ \chi_K(t_0) - \chi_{K,0} \\ \chi_K(t_0) - \chi_K(t_f) \\ \gamma_K(t_0) - \gamma_K(t_f) \end{bmatrix} = \mathbf{0}. \tag{23}$$

The additional state constraint of the initial course angle $\chi_K(t_0)$ allows to specify an initial relative wind direction of $\chi_{K,0}$. Due to the symmetry, the problem is solved only for $\chi_{K,0} \in [0°, 180°]$ with a step size of $1°$.

TAB 3. Nominal results compared to head- and tailwind condition.

	Tailwind	Nominal	Headwind
$\chi_K(t_0)$	$0\,°$	$82.55\,°$	$180\,°$
$V_{W,ref}$	$8.32\,\mathrm{m\,s^{-1}}$	$7.35\,\mathrm{m\,s^{-1}}$	$8.30\,\mathrm{m\,s^{-1}}$
$\chi_{K,Travel}$	$38.68\,°$	$56.39\,°$	$60.18\,°$
$V_{K,Travel}$	$11.99\,\mathrm{m\,s^{-1}}$	$11.23\,\mathrm{m\,s^{-1}}$	$8.56\,\mathrm{m\,s^{-1}}$
D	$94.70\,m$	$77.66\,m$	$67.87\,m$
T_{Cycle}	$7.90\,s$	$6.92\,s$	$7.93\,s$

The trajectories of the nominal, headwind, and tailwind condition are illustrated in figure 2. The direction of the wind field is indicated by the wind profile in the xz-plane. For the nominal trajectory the lift coefficient history is color-coded along the trajectory. During the lower and upper turn the maximum lift coefficient is utilized to achieve a curvature of the flight path; however, in the windward climb and leeward descent the lift coefficient decreases significantly. The angle between the positive x_N-axis and the travel direction is defined as $\chi_{K,Travel}$. For the nominal and headwind condition the travel direction is similar, whereas towards tailwinds it increases considerably. The travel speed $V_{K,Travel}$ is the downrange D (lateral euclidean distance from the initial position to the final position) per cycle time $T_{Cycle} = t_f - t_0$ and is calculated accordingly:

$$V_{K,Travel} = \frac{\sqrt{x_N(t_f)^2 + y_N(t_f)^2}}{t_f - t_0} = \frac{D}{T_{Cycle}}. \tag{24}$$

Table 3 summarizes relevant characteristic values of an energy-neutral dynamic soaring cycle for the nominal, headwind, and tailwind condition. Since the initial course angle is unconstrained in the nominal problem, the solution reveals an optimal initial course angle of $\chi_K(t_0) = 82.55°$ with respect to the given cost function in (17). Be reminded that in contrast

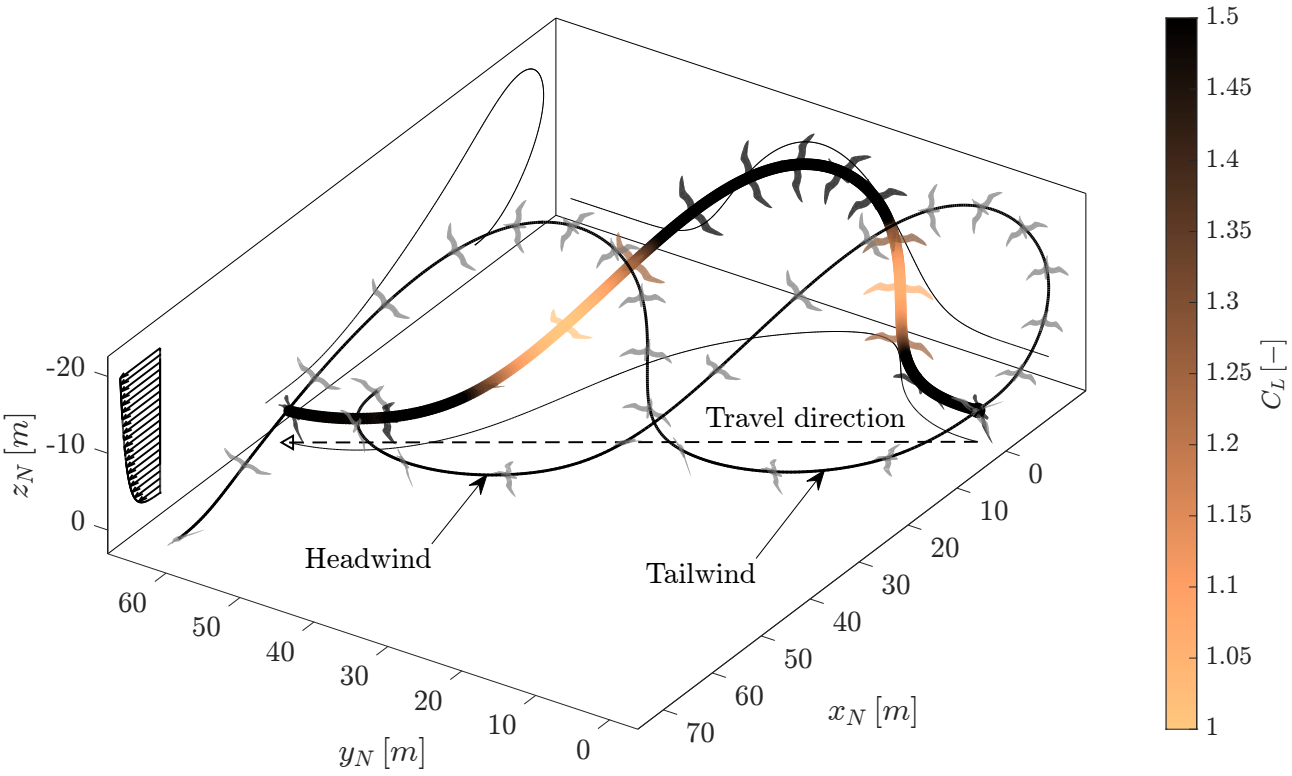

FIG 2. Trajectory of the nominal, headwind, and tailwind condition.

to the nominal case, for head- and tailwind conditions the initial course angle is prescribed and not subject to optimization. Figure 3 shows the phase diagram for the height above surface and the course angle. In the nominal case, during the lower turn for heights corresponding to $h = -z_0$, the course angle changes from roughly $49°$ to $104°$, indicated by the blue circles. Let $\mathcal{N} = \{\chi_K(t) \mid t \in [t_0, t_f],\ z_N(t) = z_0\}$ contain all course angles of the nominal trajectory for $z_N(t) = z_0$. Due to the periodicity of the maneuver, we can shift the nominal trajectory in time such that $\chi_K(t_0) = \chi_{K,N}$ and simultaneously (22) and (23) are satisfied for all $\chi_{K,N} \in \mathcal{N}$. This indicates that the time shifted solution of the nominal problem is a solution to (16) for all $\chi_{K,0} \in \mathcal{N}$. And indeed, it can be shown that the state and control histories are up to insignificant numerical deviations identical. Figure 4 shows clearly that for $\chi_{K,0} \in \mathcal{N}$ the reference wind speed is minimized to the same value of $V_{W,ref} = 7.35\,\mathrm{m\,s^{-1}}$ as in the nominal case.

Although the head- and tailwind conditions yield nearly equal reference wind speeds, their trajectories strongly diverge (see figure 2 and table 3). However, from figure 4 it is evident that tailwind conditions are generally more favorable as they require lower wind speeds for increasing crosswind components. Also, for tailwinds the travel direction changes significantly towards crosswinds, whereas for headwinds the change in travel direction is moderate (see figure 5). This becomes particularly important if it is required to travel in a certain direction relative to the wind.

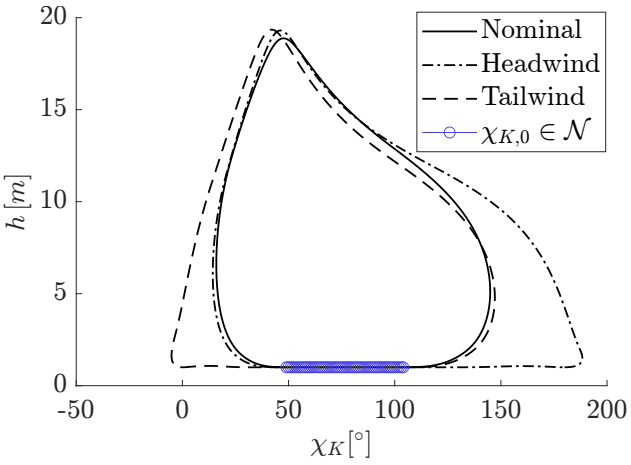

FIG 3. Height above surface over course angle for the nominal, headwind, and tailwind condition.

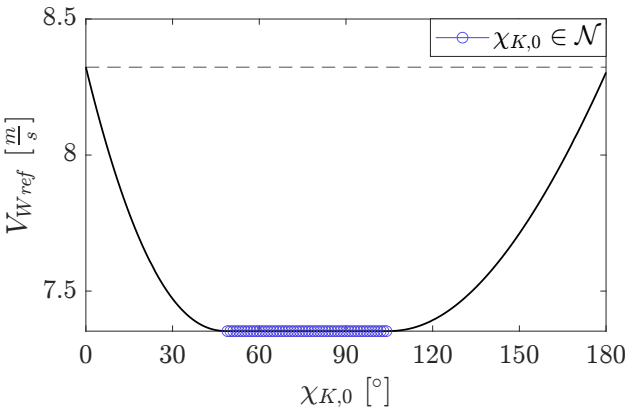

FIG 4. Minimum reference wind speed over initial relative wind direction.

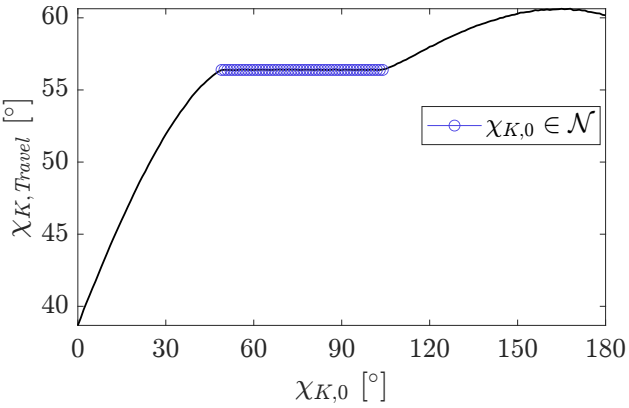

FIG 5. Travel direction over initial relative wind direction.

In headwind conditions the initial ground speed is significantly lower than in tailwind conditions (see figure 6). For the air speed the inverse analogy applies, however the differences in magnitude are less. Interestingly, the minimum air speed is almost equal for all initial relative wind directions at an air speed of approximately $V_A = 8\,\mathrm{m\,s^{-1}}$, lower than the stall speed of $V_{stall} = 11.81\,\mathrm{m\,s^{-1}}$. The minimum ground speed in tailwind conditions is slightly higher than in headwind conditions.

The control histories are shown in figure 7. It is noticeable that the structure of the lift coefficient and the bank angle does not change for different initial relative wind directions and for $\chi_{K,0} \in \mathcal{N}$ the controls equal the time shifted nominal controls.

Analogously, the cycle time, downrange, and consequently the travel speed are equivalent for $\chi_{K,0} \in \mathcal{N}$ (see figures 8a-8c). While the cycle time (see figure 8a) increases monotonically from the minima towards head- and tailwinds, the downrange and travel speed increase monotonically from headwinds to tailwinds (see figure 8b - 8c). Despite the considerable increase in downrange towards tailwinds, the gain in travel speed is alleviated by longer cycle times. While the maximum load factor hardly changes for different initial wind directions (see figure 8e), the specific energy extracted from the surrounding airflow grows towards steep head- and tailwind directions (see figure 8f).

The total specific power of the aircraft describes the energy transfer between wind and aircraft:

$$p_T(t) = V_K \left(\frac{\dot{V}_K(t)}{g_0} + \sin(\gamma_K(t)) \right). \tag{25}$$

If $p_T(t) > 0$ energy is extracted and for $p_T(t) < 0$ energy is dissipated. The total energy exchange e_T is the amount of extracted specific energy e_e plus dissipated specific energy e_d:

$$e_T = |e_e| + |e_d|. \tag{26}$$

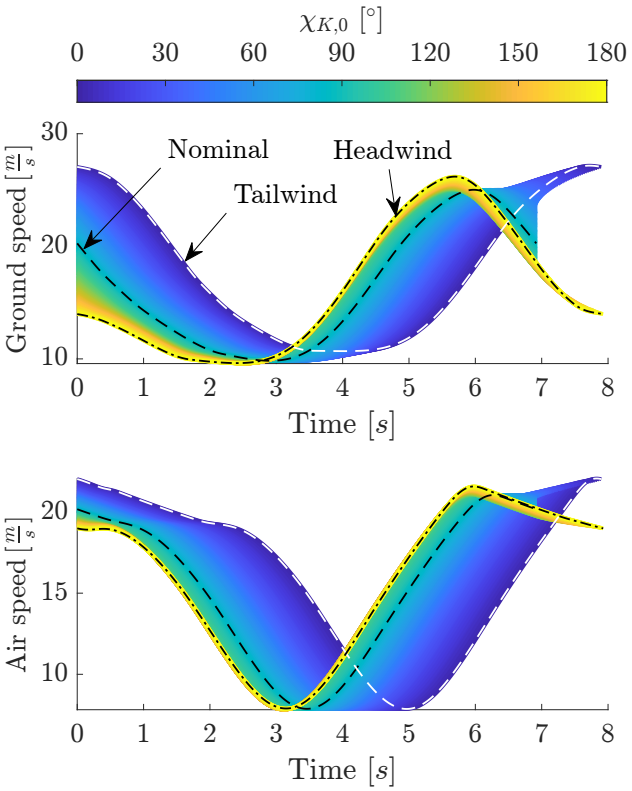

FIG 6. Ground and air speeds for varying initial relative wind directions.

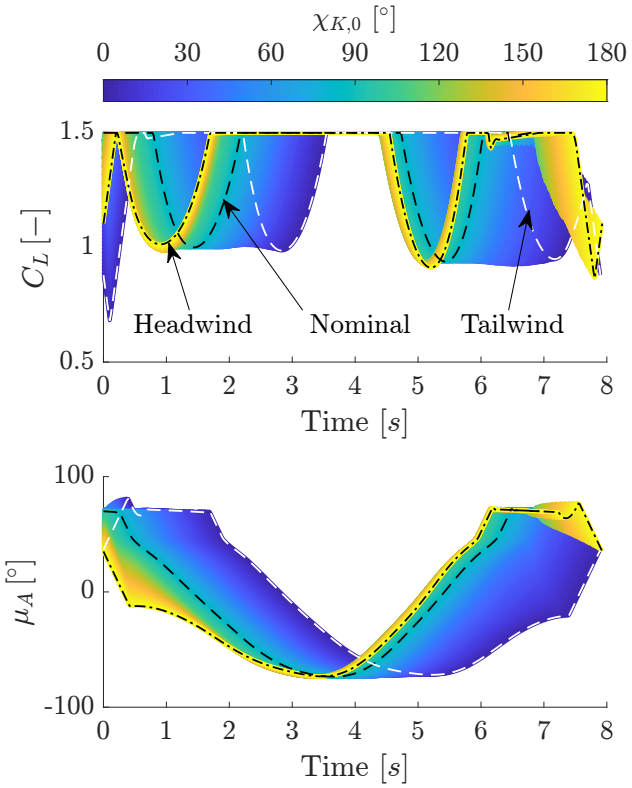

FIG 7. Controls for varying initial relative wind directions.

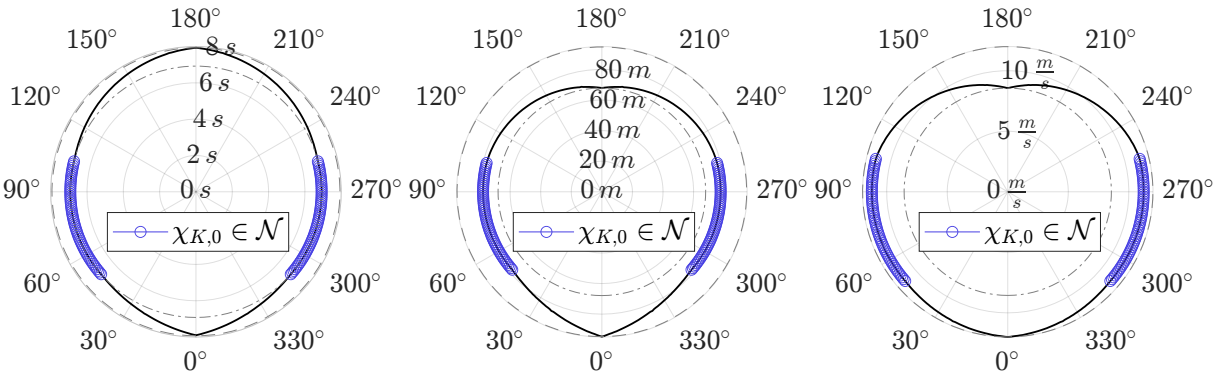

(a) Cycle time over initial relative wind direction. (b) Downrange over initial relative wind direction. (c) Travel speed over initial relative wind direction.

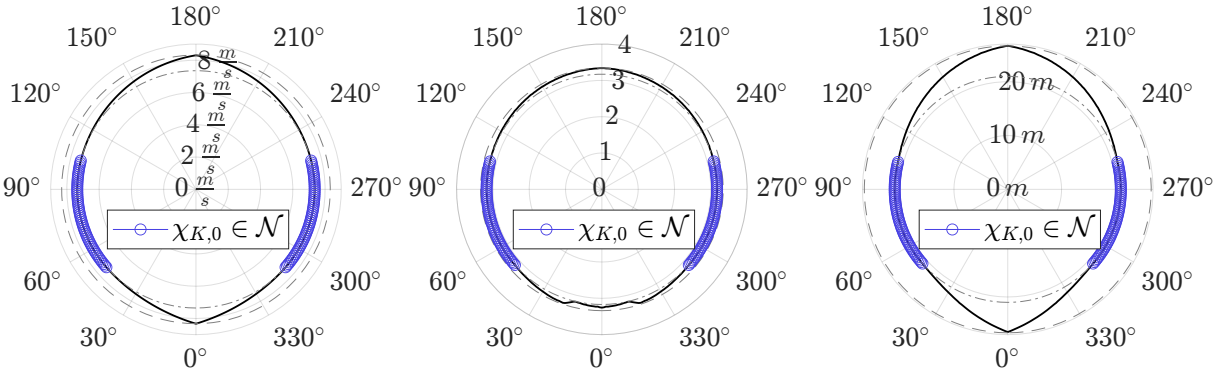

(d) Reference wind speed over initial relative wind direction. (e) Load factor over initial relative wind direction. (f) Specific extracted energy over initial relative wind direction.

FIG 8. Characteristic values for varying initial relative wind directions. The dashed and chain line represent the respective maximum and minimum values.

Thus, for an energy-neutral dynamic soaring cycle the extracted specific energy is:

$$e_e = -e_d = \frac{1}{2}\, e_T = \frac{1}{2}\int_{t_0}^{t_f} |p_T(t)|\, dt. \tag{27}$$

5. CONCLUSION

In this work, we studied the influence of the initial relative wind direction on the wind requirements of energy-neutral dynamic soaring. The investigation was accomplished by formulating a parametric optimal control problem for determining the minimum required wind reference speed for numerous initial relative wind directions and solving it numerically. The solution identified some characteristics that are helpful for the dynamic soaring practice of RPAS: The wind reference speed does not have a single optimum with respect to the initial relative wind direction. A certain range of initial directions minimizes the reference wind speed, while beyond this range, the required wind speed is higher. Besides, initial tailwind conditions are found to be more favorable in terms of downrange and travel speed. Future research will be dedicated to analyzing the influence of initial conditions for different parameters on energy-neutral dynamic soaring with higher-fidelity models and additional operational constraints.

Acknowledgement

This work was conducted in the scope of the project *RAUDY* (FKZ: 20E1910B) and funded by the Federal Republic of Germany. Funding organization: Federal Ministry for Economic Affairs and Climate Action on the basis of a decision by the German Bundestag.

Supported by:

Federal Ministry
for Economic Affairs
and Climate Action

on the basis of a decision
by the German Bundestag

Contact address:

alexander.zwenig@tum.de

References

[1] L. Rayleigh. The soaring of birds. *Nature*, 27(701):534–535, 1883. DOI: 10.1038/027534a0.

[2] L. Rayleigh. The sailing flight of the albatross. *Nature*, 40(1019):34, 1889. DOI: 10.1038/040034b0.

[3] G. Sachs, J. Traugott, A. P. Nesterova, and F. Bonadonna. Experimental verification of dynamic soaring in albatrosses. *The Journal of experimental biology*, 216(Pt 22):4222–4232, 2013. DOI: 10.1242/jeb.085209.

[4] Y. Yonehara, Y. Goto, K. Yoda, Y. Watanuki, L. C. Young, H. Weimerskirch, C. A. Bost, and Katsufumi Sato. Flight paths of seabirds soaring over the ocean surface enable measurement of fine-scale wind speed and direction. *Proceedings of the National Academy of Sciences*, 113(32):9039–9044, 2016. DOI: 10.1073/pnas.1523853113.

[5] G. Sachs. Minimum shear wind strength required for dynamic soaring of albatrosses. *Ibis*, 147(1):1–10, 2005. DOI: 10.1111/j.1474-919x.2004.00295.x.

[6] G. Sachs. Kinetic energy in dynamic soaring—inertial speed and airspeed. *Journal of Guidance, Control, and Dynamics*, 42(8):1812–1821, 2019. DOI: 10.2514/1.G003407.

[7] T. Flanzer, G. Bower, and I. Kroo. Robust trajectory optimization for dynamic soaring. In *AIAA Guidance, Navigation, and Control Conference*, Guidance, Navigation, and Control and Co-located Conferences. American Institute of Aeronautics and Astronautics, 2012. DOI: 10.2514/6.2012-4603.

[8] G. D. Bousquet, M. S. Triantafyllou, and J. J. E. Slotine. Optimal dynamic soaring consists of successive shallow arcs. *Journal of The Royal Society Interface*, 14(135):20170496, 2017. DOI: 10.1098/rsif.2017.0496.

[9] G. Sachs. Optimal force and energy management of dynamic soaring in different reference frames. In *AIAA Scitech 2020 Forum*, AIAA SciTech Forum. American Institute of Aeronautics and Astronautics, 2020. DOI: 10.2514/6.2020-1826.

[10] G. Sachs. Minimaler windbedarf für den dynamischen segelflug der albatrosse. *Journal für Ornithologie*, 134(4):435–445, 1993. DOI: 10.1007/BF01639834.

[11] M. Rieck, M. Bittner, B. Grüter, J. Diepolder, P. Piprek, C. Göttlicher, F. Schwaiger, B. Hosseini, F. Schweighofer, T. Akman, and F. Holzapfel. Falcon.m: User guide, 2022.

[12] A. Wächter and L. T. Biegler. On the implementation of an interior-point filter line-search algorithm for large-scale nonlinear programming. *Mathematical Programming*, 106(1):25–57, 2006. DOI: 10.1007/s10107-004-0559-y.

[13] United States. National Oceanic, Atmospheric Administration, and United States. Air Force. *US standard atmosphere, 1976*, volume 76. National Oceanic and Atmospheric Administration, 1976.

[14] J. T. Betts. *Practical Methods for Optimal Control and Estimation Using Nonlinear Programming, Second Edition*. Society for Industrial and Applied Mathematics, second edition, 2010. DOI: 10.1137/1.9780898718577.

[15] M. Gerdts. *Optimal Control of ODEs and DAEs*. De Gruyter, Berlin, Boston, 2011. ISBN: 9783110249996. DOI: 10.1515/9783110249996.

A. TRANSFORMATIONS

$$\boldsymbol{T}_{KN} = \begin{bmatrix} \cos(\chi_K)\cos(\gamma_K) & \cos(\gamma_K)\sin(\chi_K) & -\sin(\gamma_K) \\ -\sin(\chi_K) & \cos(\chi_K) & 0 \\ \cos(\chi_K)\sin(\gamma_K) & \sin(\chi_K)\sin(\gamma_K) & \cos(\gamma_K) \end{bmatrix}$$

$$\boldsymbol{T}_{NA} = \begin{bmatrix} a_{11} & a_{12} & a_{13} \\ a_{21} & a_{22} & a_{23} \\ a_{31} & a_{32} & a_{33} \end{bmatrix}$$

$$\begin{aligned} a_{11} &= \cos(\chi_A)\cos(\gamma_A) \\ a_{12} &= \cos(\chi_A)\sin(\gamma_A)\sin(\mu_A) - \cos(\mu_A)\sin(\chi_A) \\ a_{13} &= \sin(\chi_A)\sin(\mu_A) + \cos(\chi_A)\cos(\mu_A)\sin(\gamma_A) \\ a_{21} &= \cos(\gamma_A)\sin(\chi_A) \\ a_{22} &= \cos(\chi_A)\cos(\mu_A) + \sin(\chi_A)\sin(\gamma_A)\sin(\mu_A) \\ a_{23} &= \cos(\mu_A)\sin(\chi_A)\sin(\gamma_A) - \cos(\chi_A)\sin(\mu_A) \\ a_{31} &= -\sin(\gamma_A) \\ a_{32} &= \cos(\gamma_A)\sin(\mu_A) \\ a_{33} &= \cos(\gamma_A)\cos(\mu_A) \end{aligned}$$

The aerodynamic velocity in the local reference coordinate frame is:

$$\boldsymbol{v}_A = \begin{bmatrix} u_A & v_A & w_A \end{bmatrix}_N^{\mathsf{T}}$$

and the aerodynamic angles are determined as follows:

$$\begin{aligned} \chi_A &= \arctan\left(\frac{v_A}{u_A}\right) \\ \gamma_A &= \arcsin\left(\frac{-w_A}{V_A}\right). \end{aligned}$$